Felten, Björn; Felling, Tim; Osinski, Paul; Weber, Christoph

Working Paper

Flow-Based Market Coupling Revised - Part I: Analyses of Small- and Large-Scale Systems

HEMF Working Paper, No. 06/2019

Provided in Cooperation with:
University of Duisburg-Essen, Chair for Management Science and Energy Economics

Suggested Citation: Felten, Björn; Felling, Tim; Osinski, Paul; Weber, Christoph (2019) : Flow-Based Market Coupling Revised - Part I: Analyses of Small- and Large-Scale Systems, HEMF Working Paper, No. 06/2019, University of Duisburg-Essen, House of Energy Markets & Finance, Essen

This Version is available at:
https://hdl.handle.net/10419/201589

Flow-Based Market Coupling Revised - Part I: Analyses of Small- and Large-Scale Systems

HEMF Working Paper No. 06/2019

by

Björn Felten,
Tim Felling,
Paul Osinski
and
Christoph Weber

June 11, 2019

UNIVERSITÄT
DUISBURG
ESSEN

Open-Minded

Abstract

By interlinking power systems, significant welfare gains can be achieved. However, different approaches for coupling electricity markets exist. A recent development in this field is the implementation of flow-based market coupling (FBMC) in Central Western Europe (CWE). Indeed, FBMC has proven to be advantageous compared to the former situation in CWE Amprion et al. 2014 and to be operationally manageable under current market conditions. However, analyses of possible future adjustments of market areas ("bidding zones") have shown problems in assessing and even understanding FBMC Entso-E 2018. Therefore, Part I of this two-part paper contributes to resolving these problems. First, it presents key issues and effects of all essential FBMC elements. This is done drawing the feasible regions of the FBMC constraints – a method that is well-known from optimization theory. However, in the way it is applied to FBMC it is novel and offers significant insights. These insights are presented on the basis of a stylized yet fully transparent and reproducible example. Thereby, we improve the understanding of benefits and shortcomings of FBMC. Second, we introduce a large-scale model framework capable of assessing FBMC as implemented in CWE. This enables us to assess real-world power systems - also when undergoing structural changes. This lays the foundation for the case study presented in Part II.

Keywords : Flow-based market coupling; Zonal pricing; Nodal pricing; Feasible regions; Flow-based domains, Electricity market modeling; Grid modeling

JEL-Classification : C61, C80, D61, Q41, Q43, Q48

Björn Felten
House of Energy Markets and Finance
University of Duisburg-Essen, Germany
bjoern.felten@uni-due.de

Tim Felling
House of Energy Markets and Finance
University of Duisburg-Essen, Germany
tim.felling@uni-due.de

Paul Osinski
(Corresponding Author)
House of Energy Markets and Finance
University of Duisburg-Essen, Germany
paul.osinski@uni-due.de

Christoph Weber
House of Energy Markets and Finance
University of Duisburg-Essen, Germany
christoph.weber@uni-due.de

Contents

List of Figures

List of Tables

Abbreviations

CHP	combined heat and power.
CWE	Central Western Europe (=France, Belgium, Luxemburg, the Netherlands and Germany).
EMCP	electricity market clearing problem.
Entso-E	European Network of Transmission System Operators.
FAV	final adjustment value
FB(MC)	flow-based (market coupling).
FR	feasible region of the EMCP.
FRM	flow reliability margin.
GSK	generation shift key.
JMM	WILMAR Joint Market Model.
LFC	load flow constraint.
MC	market coupling.
NER	net export ratio.
NTC	net transfer capacity.
OPF	optimal power flow.
PTDF	power transfer distribution factor.
RES	renewable energy sources.

Nomenclature

$(e)_{0/1/2}$	considered base cases.
$\bar{A}_{f,z}$	zonal PTDF of line f for net export from zone z.
$\bar{d}_z$	aggregate demand in zone z.
$\bar{q}_z^{((e/r))}$	net exports from zone z (if with superscripts: (e) = expected at D-2 stage, (r) = realized).
$\Delta L_f^{(e)}$	expected line loading offset of line f.
$\lambda_{z,i}^{inc,(p/r)}$	GSK of node i in zone z (superscripts: (e) = expected at D-2 stage, (r) = realized).

$A_{f,i}$	PTDF of line f for net export at node i.
C_f	capacity of line f.
$c_{i/u}(g_{i/u,t})$	marginal costs of electricity generation at node i/of unit u (being a function of $g_{i/u,t}$).
d_i	demand at node i.
$e_{z,z',t}^{(component)}$	electricity exchange from price zone z (exporting) to price zone z' (importing). Components/superscripts explained in eq. 16.
$e_{z,z',t}^{max}$	net transfer capacity.
$f \in F_{(x/cb)}$	index/set of all (chosen/critical) lines.
$g_{i,t}^{res}$	non-dispatchable RES generation at node i at time t.
$g_{i/u,t}^{(component)}$	electricity generation at node i/of unit u at time t. Components/superscripts explained in table 3.
$g_{i/u,t}^{max}$	(available) electrical generation capacity at node i/of unit u at time t.
$g_{u,t}^{min}$	minimum electrical generation of unit u at time t.
$i \in I_{(z)}$	index/set of nodes of the system (if with index z: nodes within price zone z).
M_f	flow reliability margin of line f.
$q_i^{((e/r))}$	net exports at node i (if with superscripts: (e) = expected at D-2 stage, (r) = realized).
$R_f^{(n)sfd}$	remaining available margin of line f in (non-)standard flow direction.
$r_{z,i}^{abs,(e/r)}$	expected/realized net export ratio.
$t \in T^{opt}$	time stamp of the optimization period.
V_f	final adjustment value.
$z \in Z_{(FB)}$	index/set of price zones (if with index FB: zones being subject to FBMC).

1 Introduction

The design of electricity markets has been subject to vigorous debates over the last three decades. One peculiarity of electricity markets is the existence of important grid restrictions. In conjunction with the very limited storage possibilities for electricity, this makes congestion management a key issue in electricity market design. The European system has been moving towards an improved congestion management, e.g. by introducing implicit market coupling (MC). The last substantial move in that direction has been the introduction of flow-based MC (FBMC) for the electricity markets in Central West Europe (CWE, i.e. France, Belgium, Luxemburg, the Netherlands and Germany) in May 2015.

In order to assess and further develop the European electricity markets, tools are needed that can quantify the effect of potential policy and market design changes under use of this state-of-the-art MC method. Therefore, the paper at hand introduces a large-scale model framework that is capable of reproducing all stages of the MC process to a high level of detail; starting with the processes of capacity allocation, proceeding with the clearing of the European day-ahead and intraday markets, and finishing with potentially necessary redispatch measures. The high level of accuracy is achieved by three types of activities: (i) resorting to proven large-scale program tools specialized in grid and market modeling (i.e. MATPOWER [Zimmermann et al. 2011] and the Joint Market Model (JMM) [Meibom et al. 2006; Weber et al. 2009] incl. its CHP tool [Felten et al. 2017]), (ii) developing program enhancements allowing to model all abovementioned FBMC stages and (iii) implementing tailored data handling routines in order to use consistent input data at different levels of aggregation and to hand over all necessary data between the program stages. With regard to MC procedures, special attention is paid to the fact that, throughout Europe, different methods of MC coexist. In particular, the NTC-based MC is still in use outside of CWE and, thus, it is an important feature of our model to be capable of replicating both MC mechanisms in a combined manner. In addition to model developments related to FBMC, for a comprehensive view on MC efficiency, redispatch must be taken into account. Therefore, a capacious redispatch tool has been developed [Felling et al. 2019].

Recently, some model-based assessments of FBMC have been developed by further researchers [Finck et al. 2018; Marjanovic et al. 2018; Sebestyén et al. 2018; Wyrwoll et al. 2018]. Some of these assessments deal with a comparison of NTC-based market coupling and FBMC in Central Eastern Europe [Marjanovic et al. 2018; Finck et al. 2018], others analyze the impact of FBMC procedures on exchange flows / trading volumes [Wyrwoll et al. 2018] or market clearing results [Sebestyén et al. 2018]. The paper at hand and its companion exceed the abovementioned papers in various aspects: First, we focus our analyses on the welfare resulting from the entire FBMC process. This does not only include the (day-ahead and intraday) market clearing, it also considers redispatch amounts and costs. Second, we scrutinize the process-inherent inadequacies of FBMC in detail. Therefore, we develop novel illustrations of the FBMC domain and describe the cause-and-effect relations of FBMC approximations. These analytical insights are taken up in [Felling et al. 2019] where the respective inaccuracies are assessed based on a

large-scale model. Third, our model uses a holistic approach modeling all relevant European markets being coupled by distinct MC mechanisms and enabling a high level of detail by the combined use of specialized tools. Only by means of such detailed fundamental models, the potential effects of structural changes to European electricity market design can be quantified. Thus, the developments constitute a significant contribution in terms of electricity market analysis. Forth, our analyses and large-scale model developments are used to perform a case study of improved price zone configurations. This constitutes a significant novelty compared to all of the abovementioned papers.

In order to interpret results of large-scale models, it has proven very useful to first analyze cause-and-effect relations of added model features on the basis of stylized (or small-scale) examples. Thus, before explaining the large-scale model, our paper illustrates the effect of essential FBMC elements by contrasting the feasible region (FR) under FBMC with the physical grid constaints. As these physical constraints are considered in nodal market designs, our stylized analysis can be seen as a zonal-vs.-nodal assessment. Such comparative studies are not new. Existing studies usually solve the electricity market clearing problems (EMCPs) under both market designs (zonal and nodal). E.g. by assessing resulting differences in welfare, the effectiveness of the market designs can then be compared. In the assessments of the nodal market designs, the consideration of load flow constraints (LFCs) of transmission lines is quite similar in all studies, as it constitutes the straightforward translation of physical properties of the grid. This is not the case for zonal market designs, and existing studies differ in this regard. Based on how LFCs are considered in zonal market designs, two groups of studies may be distinguished:

Nodal knowledge Load flows are calculated based on information on power injections/withdrawals at nodal level and using individual line sensitivities. Thus, the state of the power system is known and considered at a highest possible spatial granularity. The way how the MC considers zone delimitations can vary. In some cases, explicit price equality constraints within zones are added to the EMCP (e.g. in [Bjørndal and Jörnsten 2001; Ehrenmann and Smeers 2005; Bjørndal and Jörnsten 2007; Androcec and Krajcar 2012]). In other cases, intra-zonal LFCs are excluded from the EMCP (e.g. in [Bjørndal et al. 2003; Grimm et al. 2016; Grimm et al. (2) 2016]). In latter cases, the limit values for load flows on inter-zonal lines may be downsized to prevent intra-zonal congestion (cf. [Bjørndal et al. 2003]).

Aggregated grid Load flows or exchanges across borders are aggregated (cf. [Ehrenmann and Smeers 2005; Oggioni and Smeers 2013; Neuhoff et al. 2013; Grimm et al. 2016]). For approximating load flows and line constraints, aggregated grid models are used, which only consider demand and supply balances at zonal level - i.e. at a much lower spatial resolution than the MC mechanisms under a). The limit values for these flows are sometimes determined by summing up line capacities or by other operations (cf. [Ehrenmann and Smeers 2005]). Frequently, constraints of the EMCP are not imposed on aggregated physical values (i.e. load flows) but on commercial transactions (i.e. bilateral exchanges, cf. [Oggioni and Smeers 2013;

Neuhoff et al. 2013; Grimm et al. 2016]). This special case of constraint formulation implies that only "sensitivity" factors of zeros and ones are used. Latter design corresponds to NTC-based MC.

All of these studies have greatly contributed to the discourse on zonal market designs. E.g. [Bjørndal and Jörnsten 2001] and [Ehrenmann and Smeers 2005] reveal significant shortcomings (notably welfare losses) of several zonal market designs. Yet, since the publication of these papers, the transmission system operators (TSOs) in CWE, regulatory authorities and other involved parties have made considerable efforts setting up the FBMC methodology and elaborating its procedures. Some relevant design choices have been made for FBMC: The consideration of individual lines (i.e. no aggregated grid representation) which also includes selected intra-zonal lines, the use of so-called generation shift keys (GSKs), the consideration of a base case, the use of flow reliability margins (FRMs) and the nonconsideration of bids and asks at nodal level (i.e. no nodal knowledge). Due to these elaborate procedures, certain improvements compared to the early concepts of MC can be expected and revisiting the zonal market design with focus on the essential FBMC concepts seems expedient. As a matter of fact, there is even an evident need for such analyses, as the European Network of Transmission System Operators (Entso-E) has encountered *"non-resolvable complexities"* during the course of its Bidding Zone Study [Entso-E 2018]. To a great extent, the complexities mentioned by Entso-E refer to *"essential market design features (especially regarding the design of the capacity calculation approach, e.g. base case approach, CBCO selection, GSK strategy)"*. Therefore, we present a novel approach of analyzing all these FBMC features. We design a transparent and reproducible example which allows us to give a full description of the FR of the zonal EMCP and contrasting it with subspaces of the nodal FR. Both, the consideration of essential FBMC concepts in zonal-vs.-nodal analyses and the novel and clear-cut illustration, distinguish our paper from existing literature. Having said that, there is some body of literature on FBMC. Apart from Entso-E procedures, descriptive papers on FBMC [Plancke et al. 2016; Van den Bergh et al. 2016] exist. Such descriptions are sometimes extended by statistical assessments [Jegleim 2015; Morin 2016]. However, none of these papers illustrates the effects of the elements of FBMC in a clear analytical way nor do they contain a large-scale fundamental model that could replicate real-world processes or FBMC procedures.

This paper is structured as follows: Sec. 2 provides a short summary of the theoretical background. It explains the equations describing the physical constraints of the power system and the LFCs considered under FBMC. Subsequently, sec. 3 illustrates cause and effect of the essential elements of the FBMC methodology based on a stylized example. Then, sec. 4 builds the bridge from small-scale to large-scale modeling. Hence, the large-scale model framework is introduced, the representation of real-world restrictions is explained (also comparing it with that of small-scale models), and the combined modeling of FBMC and NTC-based MC is presented. Thereafter, sec. 5 draws the relevant conclusions.

2 Theoretical Background

From an economic point of view, the maximization of social welfare is generally seen as the key objective when designing electricity markets. In the absence of price elasticity of demand, maximizing welfare corresponds to an optimization problem that minimizes operational system costs under several constraints. This statement equally holds for nodal and zonal market designs. However, in terms of formulating the constraints of power flows through the electricity grid (i.e. LFCs), both market designs differ substantially. The conceptual differences are explained subsequently.

2.1 Representation of Physical Behavior of Line Loads and Restrictions - The Nodal Market Design

The nodal EMCP is given in eq. 1 to 5. Therein, eq. 1 represents the objective function, and g_i is the aggregate generation at each grid node i. c_i are the corresponding marginal costs, which depend on the actual generation. I represents the set of all nodes of the system. Eq. 2 represents the LFCs. Here, $A_{f,i}$ is the power transfer distribution factor (PTDF) for the loading of line f resulting from an exchange from node i to an (arbitrary) reference node.[1] C_f is the line capacity. q_i is the net export at node i, which is simply the balance of generation g_i and demand d_i (eq. 3). The solution to the optimization problem remains unchanged if noncritical lines are removed from the set of considered lines F_x. The resulting set of critical lines includes all lines whose capacity restriction becomes binding at least in one situation. Eq. 4 assures that generation and demand of the overall system are in balance, eq. 5 expresses the capacity constraints of the generators.

$$\min_{g_i} \quad \sum_{i \in I} c_i(g_i) g_i \tag{1}$$

$$s.t. \qquad -C_f \leq \sum_{i \in I} A_{f,i} q_i \leq C_f \qquad \forall\, f \in F_x \tag{2}$$

$$q_i = g_i - d_i \qquad \forall\, i \in I \tag{3}$$

$$\sum_{i \in I} q_i = 0 \tag{4}$$

$$0 \leq g_i \leq g_i^{max} \qquad \forall\, i \in I \tag{5}$$

Eq. 1 to 5 constitute a nodal EMCP. Moreover, as the LFCs of this nodal EMCP (eq. 2) consider the actual line loading behavior quite precisely, they can be regarded as physical grid constraints. These nodal LFCs always need to be fulfilled - no matter if the market design is nodal or zonal.

[1] PTDFs express the line loading sensitivity in terms of net exports. We limit the illustration to the DC lossless load flow approximation (cf. [Zimmermann et al. 2011]).

2.2 Zonal Pricing Using CWE-style FBMC

For understanding FBMC, it is important to be aware of the sequential character of FBMC. The left column of fig. 1 illustrates the main stages of the FBMC process. Two days before delivery (D-2), the capacity allocation takes place, i.e. the TSOs determine the parameters which define how much cross-zonal trade is allowable. These grid-based input parameters are used in the 2nd stage (D-1), when the day-ahead market is cleared. This clearing aims at a welfare-optimal use of available exchange capacities. At D-1, the EMCP as shown in eq. 6 to 10 is solved.

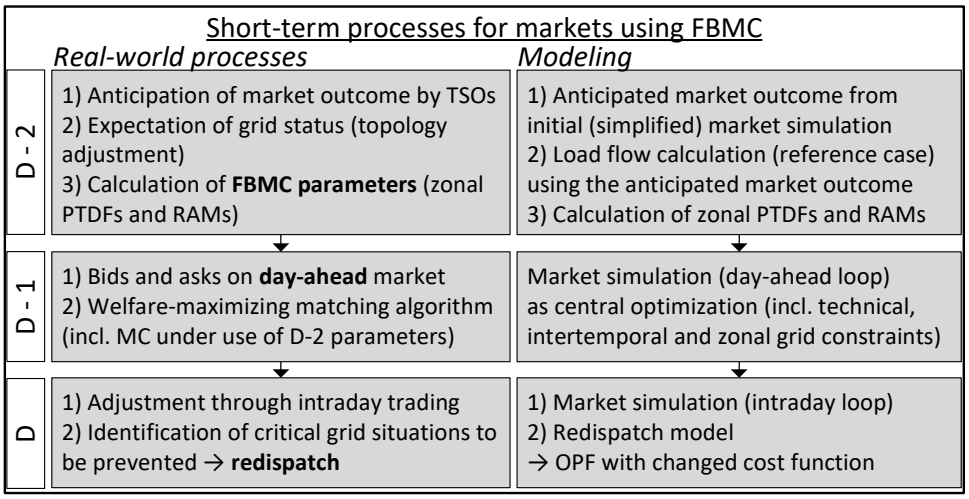

Figure 1: Illustration of real-world processes and the corresponding modeling.

In contrast to section 2.1, we now assume that the system is composed of a set of price zones Z. Each zone z contains a set of nodes I_z. This optimization problem is quite similar to the nodal EMCP; i.e., the objective function, system balance equation and capacity constraints of the generators remain unchanged. The main difference is that only the net exports at the level of price zones, $\bar{q}_z$, are taken into account (eq. 8) and, thus, only these are constrained (eq. 7). This entails two conceptual changes. First, the sensitivity of loading line f resulting from an exchange from zone z (instead of node i in the nodal design) to a reference node must be used. Accordingly, the PTDFs are used in their zonal form $\bar{A}_{f,z}$. The second conceptual change is the use of remaining available margins (RAMs) $R_f^{nsfd/sfd}$ as limit values in eq. 7. The calculation of $\bar{A}_{f,z}$ and $R_f^{nsfd/sfd}$ and the choice of F_{cb} are explained below.

$$\min_{g_i} \quad \sum_{i \in I} c_i(g_i) g_i \tag{6}$$

$$s.t. \qquad R_f^{nsfd} \leq \sum_{z \in Z} \bar{A}_{f,z} \bar{q}_z \leq R_f^{sfd} \qquad \forall\, f \in F_{cb} \tag{7}$$

$$\bar{q}_z = \sum_{i \in I_z} g_i - \sum_{i \in I_z} d_i \qquad \forall\, z \in Z \tag{8}$$

$$\sum_{z \in Z} \bar{q}_z = 0 \tag{9}$$

$$0 \leq g_i \leq g_i^{max} \qquad \forall\, i \in I \tag{10}$$

2.2.1 The zonal PTDF $\bar{A}_{f,z}$

For translating nodal to zonal PTDFs, certain approximations must be made. Key elements for calculating $\bar{A}_{f,z}$ are the GSKs $\lambda_{z,i}^{inc,(p)}$.

$$\bar{A}_{f,z} = \sum_{i \in I_z} \lambda_{z,i}^{inc,(p)} A_{f,i} \quad \text{with} \sum_{i \in I_z} \lambda_{z,i}^{inc,(p)} = 1 \tag{11}$$

Mathematically, the calculation is simply a weighted average of nodal PTDFs with GSKs being the weights. By regarding eq. 2, 7 and 11, the interpretation of GSKs becomes apparent: GSKs are used to distribute a change in net exports of a zone $\Delta\bar{q}_z$ to nodes within that zone, i.e. allocating changes in net exports to these nodes ($\Delta\bar{q}_z \overset{GSK}{\longrightarrow} \Delta q_i$). From eq. 11, it is not straightforward why the allocation by means of GSKs refers to changes in zonal net exports (i.e. $\Delta\bar{q}_z$ to Δq_i) instead of absolute net exports (i.e. $\bar{q}_z$ to q_i). We come back to this point in the next paragraph.

2.2.2 The Remaining Available Margin $R_f^{nsfd/sfd}$

RAMs consist of four elements; the line capacity C_f, the line load offset $\Delta L_f^{(e)}$, the FRM M_f and the final adjustment value (FAV) V_f. They are distinguished by flow direction: standard flow direction (superscript sfd) and non-standard flow direction (superscript $nsfd$).

$$R_f^{sfd} = C_f - \Delta L_f^{(e)} - M_f - V_f \tag{12}$$

$$R_f^{nsfd} = -C_f - \Delta L_f^{(e)} + M_f + V_f \tag{13}$$

$\Delta L_f^{(e)}$ consider the base case net exports $q_i^{(e)}$. Such a base case represents a best estimate of the power system for the day of delivery (D). We superscribe values that are dependent on this base case expectation with (e). If any of the expected $q_i^{(e)}$s is non-zero, the expected line loading of at least one line is unequal to 0. The expected line loadings reduce the free line capacity. They are given by $\sum_{i \in I} A_{f,i} q_i^{(e)}$. Using a base case also implies that changes in line loading result from deviations of zonal net exports from the base case (i.e. from $\Delta\bar{q}_z = \bar{q}_z - \bar{q}_z^{(e)}$). However, eq. 7 only contains $\bar{q}_z$ in its inner term, since the expected part ($\sum_{z \in Z} \bar{A}_{f,z} \bar{q}_z^{(e)}$) is shifted to the left and right side of eq. 7. From the EMCP perspective, this part is constant (since it is predetermined) and, therefore, is contained in the RAMs. Thus, $\Delta L_f^{(e)}$ is calculated as follows.

$$\begin{aligned} \Delta L_f^{(e)} &= \sum_{i \in I} A_{f,i} q_i^{(e)} - \sum_{z \in Z} \bar{A}_{f,z} \bar{q}_z^{(e)} \\ &= \sum_{z \in Z} \sum_{i \in I_z} A_{f,i} \left(q_i^{(e)} - \lambda_{z,i}^{inc,(p)} \bar{q}_z^{(e)} \right) \end{aligned} \tag{14}$$

The purpose of the base case is explained in sec. 3.3. However, its use is the reason for the incremental character of GSKs, i.e. why GSKs map incremental changes ($\Delta\bar{q}_z = \bar{q}_z - \bar{q}_z^{(e)} \overset{GSK}{\longrightarrow}$

$\Delta q_i = q_i - \bar{q}_i^{(e)}$). This becomes clear when inserting eq. 12 together with eq. 14 and eq. 11 into the LFC in SFD in eq. 7. After slight rearrangements, this then reads:

$$\begin{aligned} &\sum_{z \in Z} \sum_{i \in I_z} A_{f,i} \lambda_{z,i}^{inc,(p)} \left(\bar{q}_z - \bar{q}_z^{(e)} \right) \\ &\leq C_f - \sum_{i \in I} A_{f,i} q_i^{(e)} - M_f - V_f \end{aligned} \tag{15}$$

In turn, this incremental characteristic makes it the only reasonable choice to limit $\lambda_{z,i}^{inc,(p)}$ to positive values. I.e. it would not be reasonable to expect generators at a node to decrease their generation while the overall generation in that zone increases.[2] Notably, the resulting range from 0 to 1 for all GSKs is also respected by procedures in public GSK guidelines (cf. sec. 2.2.5).

2.2.3 FRMs and FAVs

The third term for calculating the RAM is the FRM. For now, it is sufficient to note that FRMs exist, i.e. some sort of margin which can only make zonal LFCs more restrictive ($M_f \geq 0$). Its motivation and a numerical example are provided in sec. 3.6. The FAVs are partly different. They can be positive, accounting for additional risk of overload, or negative, accounting for complex remedial actions (cf. [Amprion et al. 2014]). Positive FAVs act in an identical manner as FRMs. Negative FAVs are very specific to the set of available control elements of the grid. FAVs are not included in the aforementioned *"non-resolvable complexities"* of FBMC (cf. [Entso-E 2018]) and, therefore, not in the focus of this paper. However, we briefly comment on this aspect in sec. 3.5.

2.2.4 Considered lines

Whether the set of considered lines F_{cb} contains all lines F or a subset, is a matter of choice. TSO guidelines for this choice and parameter calculations are explained subsequently. The reasons for/against considering intra-zonal lines in the EMCP are explained in sec. 3.5.

2.2.5 TSO procedures for D-2 calculations

It is important to keep in mind that all of the aforementioned FBMC elements, namely GSKs $\lambda_{z,i}^{(p)}$, base case and resulting $\Delta L_f^{(e)}$, FRMs, FAVs and the set F_{cb} of considered lines, must be defined/determined at the D-2 stage (or earlier). TSOs have published several procedures/guidelines in this regard. In terms of GSKs, Entso-E [Entso-E 2016] proposes quite unsophisticated

[2] In terms of the demand, the reason for limiting $\lambda_{z,i}^{inc,(p)}$ at 0 and 1 is the high spatial correlation of main drivers of electric demand (cf. [Xie and Hong 2016; Ziel and Liu 2016]).

calculation methods. For instance, GSKs can be calculated being proportional to the base case generation, proportional to remaining available capacity or depending upon a merit order list. In practice, further calculation methods are used. Most frequently, GSK values reciprocal to the number of nodes in a zone or proportional to installed capacities are encountered in practice (cf. [Dierstein 2017]).[3] We consider all of these procedures to be rule-based rather than representing an expectation. Therefore, we superscribe the GSK parameters - as used in FBMC - with (p) for "predetermined" instead of (e) for "expected".

The determination of the base case is described in [Amprion et al. 2014] and [Elia 2015]. In short, participating TSOs elaborate 2-day-ahead congestion forecasts. These represent best estimates of the state of the power system at day D. Several of the input parameters are taken from an agreed reference day (e.g. net exchange programs, generation of units) and are adjusted according to, amongst others, load, renewables and outage forecasts.

In terms of considered lines, all inter-zonal lines and some intra-zonal lines are considered in the EMCP. TSOs have determined a threshold for considering intra-zonal lines: If the maximum zone-to-zone PTDF[4] of a line is higher than 0.05, the line is considered to be significant (cf. [Amprion et al. 2014]).

[3] Note that statistical procedures were proposed recently (cf. [Schönheit and Sikora 2018]). However, they have yet to be validated and tested.

[4] A zone-to-zone PTDF is given by $\bar{A}_{f,z} - \bar{A}_{z',t}$ for two zones z and z'.

3 Understanding the FBMC Elements

3.1 Stylized Example

For showing the effects of all these FBMC elements, we consider the stylized 4-node examples shown in fig. 2 and 3. The physical system in both figures is identical (cf. line properties in table 1 and resulting PTDFs in table 2). The only difference is the market design. In fig. 2, it is a nodal pricing design, i.e. each node constitutes a separate price zone. In fig. 3, nodes 2 and 3 are assigned to one common zone BC. Here, zonal pricing using the CWE-style FBMC approach is supposed (cf. eq. 6 to 14).

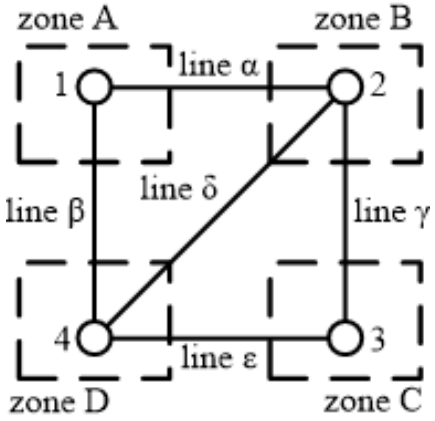

Figure 2: Stylized example under a nodal pricing regime.

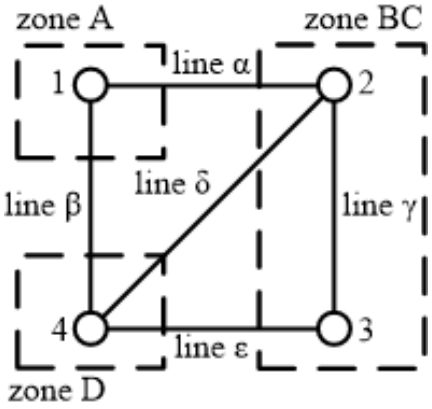

Figure 3: Stylized example under a zonal pricing regime.

Table 1: Line properties for the chosen example.

line f:	α	β	γ	δ	ϵ
line capacity C_f [MW] :	75	75	130	50	130
line reactance [Ω]:	50	50	50	50	50

Table 2: PTDFs with reference node 3 (positive flow direction (SFD) going to the node with higher numeral, $\bar{A}_{f,BC}$ for $\lambda^{inc,(p)}_{BC,2}$=0.8).

export at node	1	2	3	4	from zone	BC
$A_{\alpha,i}$ [-]	0.5	-0.125	0	0.125	$\bar{A}_{\alpha,BC}$	-0.1
$A_{\beta,i}$ [-]	0.5	0.125	0	-0.125	$\bar{A}_{\beta,BC}$	0.1
$A_{\gamma,i}$ [-]	0.5	0.625	0	0.375	$\bar{A}_{\gamma,BC}$	0.5
$A_{\delta,i}$ [-]	0	0.25	0	-0.25	$\bar{A}_{\delta,BC}$	0.2
$A_{\epsilon,i}$ [-]	-0.5	-0.375	0	-0.625	$\bar{A}_{\epsilon,BC}$	-0.3

3.2 Concepts and Conventions for the Analyses

In sec. 3.3 to 3.6, we explain the cause and effect of the essential FBMC elements by analyzing the feasible regions (FRs) of the zonal EMCP and contrasting them with subspaces of the nodal FR. For all explanations, we assume infinite power plant capacities (i.e. eq. 5 and 10 are rendered irrelevant). Our focus is on situations with scarce exchange capacities (i.e. at least one binding LFC). The FRs are always shown in the q_1-q_4 plane. With the zonal EMCP containing three variables q_1, q_4 and $\bar{q}_{BC}$, out of which only two are independent due to eq. 9, the zonal FR is fully defined in the q_1-q_4 plane.[5] The nodal EMCP contains three free variables. Therefore, only subspaces of the nodal FR can be depicted unequivocally in any 2D illustration. Prior to explaining the way of defining these subspaces, we introduce the following definitions:

- $\lambda_{z,i}^{inc,(p)}$: The incremental and predetermined GSK as used in FBMC (cf. sec. 2.2.1 and 2.2.2).
- $r_{z,i}^{abs,(e)}$: The expected net export ratio (NER), i.e. the ratio of nodal to zonal net exports. The term "expected" indicates that the NER is (implicitly) given by the base case expectation. Thus, $r_{z,i}^{abs,(e)}$ is equal to $q_i^{(e)}/\bar{q}_z^{(e)}$.
- $r_{z,i}^{abs,(r)}$: The realized NER. The term "realized" points to an ex-post perspective. Knowing the result of an EMCP (superscript (r)) allows to calculate the realized NER. It can be constructed from any feasible solution of the nodal EMCP with $\bar{q}_z \neq 0$.
- $\lambda_{z,i}^{inc,(r)}$: The incremental realized GSK. Again, we use an ex-post perspective. In contrast to $r_{z,i}^{abs,(r)}$, $\lambda_{z,i}^{inc,(r)}$ is now calculated using the deviations of net exports from the base case expectation ($= \frac{q_i^{(r)}-q_i^{(e)}}{\bar{q}_z^{(r)}-\bar{q}_z^{(e)}}$).

As explained, $\lambda_{z,i}^{inc,(p)}$ ranges from 0 to 1. For all our examples, we arbitrarily choose $\lambda_{BC,2}^{inc,(p)}$=0.8. In turn, NERs and $\lambda_{BC,2}^{inc,(r)}$ may also take values greater than 1 or less than 0, which is further described in sec. 3.3. Notably, both realized values, $\lambda_{BC,2}^{inc,(r)}$ and $r_{BC,2}^{abs,(r)}$, are used for defining subspaces of the nodal FR. We have chosen to use these elements because of their similarity to $\lambda_{BC,2}^{inc,(p)}$. However, it is important to note that $\lambda_{BC,2}^{inc,(p)}$ is the only parameter used in FBMC. In particular, neither $\lambda_{BC,2}^{inc,(r)}$ nor $r_{BC,2}^{inc,(r)}$ are defined ex ante and do not impose any restriction to the nodal FR. That is to say, the actual nodal FR is composed of a multitude of subspaces like those being illustrated subsequently. Furthermore, $\lambda_{BC,2}^{inc,(r)}$ is computed with reference to a base case. However, the base case concept does not exist in nodal designs, as solving the nodal EMCP is done in one single step. Thus, $\lambda_{BC,2}^{inc,(r)}$ and $r_{BC,2}^{abs,(e/r)}$ are concepts exclusively used for visualization, which ought not to be confused with a reduced flexibility of the nodal EMCP.

[5] Note that this aspect distinguishes our illustrations from common TSO-style depiction (e.g., in [Plancke et al. 2016]), which depict subspaces of the zonal FR in terms of bilateral exchanges.

3.3 Use and Effect of GSKs

In order to analyze the influence of GSKs, we start by considering the base case $(e)_0$ being defined as $q_i^{(e)} = 0 \; \forall \; i \in I$. The black dashed lines in fig. 4 represent the LFCs of the zonal EMCP ($\lambda_{BC,2}^{inc,(p)}$=0.8). The parts of the LFCs which define the zonal FR are highlighted in bold and black. To illustrate possible solutions that a nodal EMCP may take, we consider two possible realizations of $\lambda_{BC,2}^{inc,(r)}$ ($=r_{BC,2}^{abs,(r)}$ for $(e)_0$): 0 (red and dash-dotted) and 1 (blue and dotted). The subspaces of the nodal FR are highlighted in bold using the same color scheme as for the corresponding LFCs.

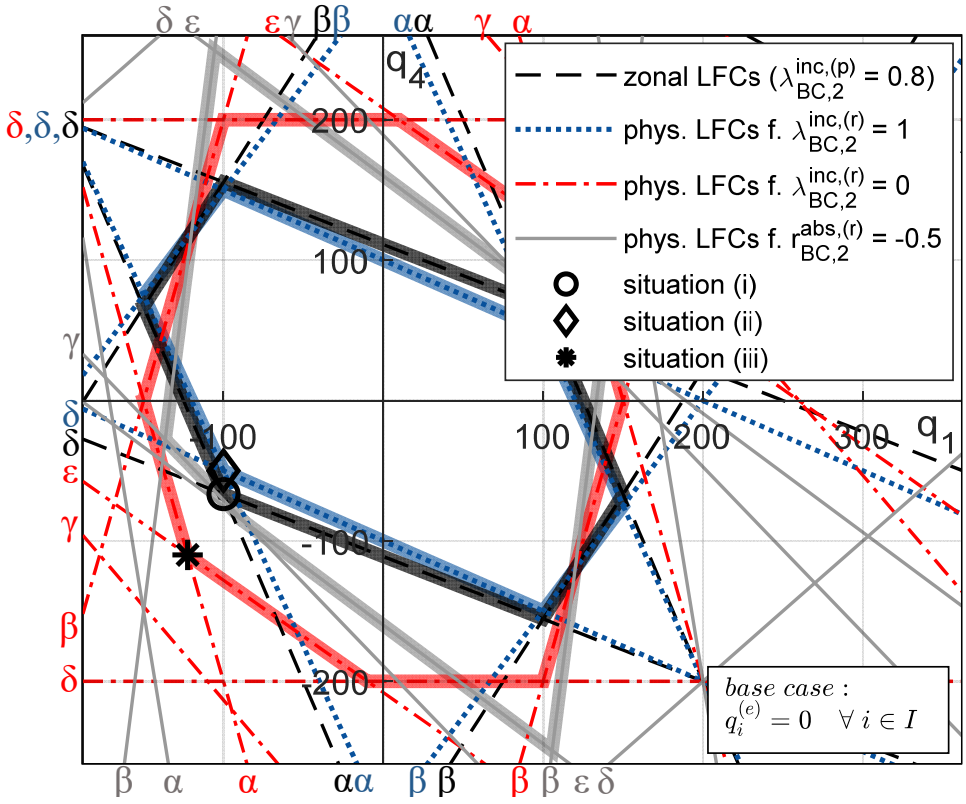

Figure 4: LFCs of the zonal and nodal EMCP for the 4-node example under a zero base case (for the nodal EMCP, three realizations are shown)

In fig. 4, we also point to some specific exchange situations, which we discuss as follows. Assume that the solution of the zonal EMCP corresponds to situation (i). In a nodal EMCP, the welfare-optimal solution may be different. Such a solution can be described by q_1, q_4, $(e)_0$ and $\lambda_{BC,2}^{inc,(r)}$. Then, any deviation of $\lambda_{BC,2}^{inc,(r)}$ from $\lambda_{BC,2}^{inc,(p)}$ changes the optimal feasible exchange. Subsequently, we discuss the expected solution, the two further possible GSK realizations and the consequences of their divergence:

Zonal solution with $\lambda_{BC,2}^{inc,(p)}$=0.8 The solution of the zonal EMCP is given at $\bar{q}_{BC}$=166.7 MW. This corresponds to q_1=-100 MW and q_4=- 66.7 MW (situation (i) in fig. 4). At this

point, lines α and δ are expected to be critical, i.e. entirely loaded. If $\lambda_{BC,2}^{inc,(r)}$ is identical to its expectation (0.8), then situation (i) also represents the nodal solution in our stylized example. Thus, the zonal solution would be welfare-optimal, and redispatch is not required on the day of delivery.

$\lambda_{BC,2}^{inc,(r)}$=1, i.e. all net exports of zone BC stem from node 2 q_2 has a stronger impact on both critical line loadings (of lines α and δ) than q_3. Therefore, the zonal solution ($\bar{q}_{BC}$=166.7 MW) breaches either one or both of these technical constraints (α and/or δ). Hence, the solution of the zonal EMCP would make redispatch necessary. Assume that the optimal solution under adequate consideration of technical constraints would then be the one given at situation (ii), i.e. q_1=-100 MW, q_4=-50 MW and, thus, $\bar{q}_{BC}$=150 MW. Taking the zonal solution as starting point (as it is the outcome of the D-1 stage under FBMC, cf. item a)), the optimal solution (ii) could only be achieved by negative redispatch at node 2 and positive redispatch at node 4. Alternatively, technical feasibility could be established by intra-zonal redispatch at nodes 2 and 3. However, this alternative redispatch will not yield a welfare-optimal result. Thus, resulting welfare depends on the way redispatch is performed.

$\lambda_{BC,2}^{inc,(r)}$=0, i.e. all net exports of zone BC stem from node 3 As q_3 has a weaker impact on both critical line loadings than q_2, higher net exports from zone BC would be permissible. As a matter of fact, the set of critical lines even changes (from α and δ in situation (i) to e.g. α and ϵ in situation (iii)). Again, the solution of the zonal EMCP (situation (i)) is suboptimal – in this case, because as some available line capacities remain unused.

For different market situations, the direction of exchanges and, correspondingly, the point of highest welfare may be different. Yet, in case of scarce exchange capacities, the effects of GSK inaccuracy will be throughout similar to the ones described above.

In fig. 4, we also show physical LFCs for $r_{BC,2}^{abs,(r)}$=-0.5 (grey solid lines). A negative NER can occur, for instance, when some nodes in a zone are net exporters (e.g. surplus of low-cost generation capacities) while other nodes in the same zone are net importers (e.g. no generation capacities). If the zonal net export is positive, this results in a negative NER for the importing node. Implicitly, part of the generation at the exporting nodes is balanced with the demand at importing nodes, which is equivalent to (implicit) intra-zonal trade. In the regarded case, most of the electricity traded between node 3 and 2 is transmitted through the intra-zonal line γ, thereby reducing its free capacity for cross-zonal trade.[6] A smaller part takes indirect routes through the grid.

Even if all zonal net exports are 0, lines may be loaded if there are exchanges between nodes within one zone. As indicated by the PTDF matrix, there will then also be flows through other parts of the grid - these are the so-called loop flows [Elia 2017]. The inner term of eq. 7 does

[6] More specifically, PTDFs in table 2 show that transmission corresponds to 62.5% of such trades. Thus, the LFCs of line γ can become relevant (i.e. possibly binding) for situations with $r_{BC,2}^{abs,(r)}$=-0.5, as can be seen in fig. 4.

not take into account intra-zonal trade. Yet, their impact on the line loadings is contained in the term $\Delta L_f^{(e)}$. Describing the impact of intra-zonal trade on line loadings is hence one major purpose of the base case.

3.4 Use and Effect of the Base Case

Following the previous considerations, we now relax the initial assumption of all $q_i^{(e)}$ being equal to 0. Mathematically, this results in $\Delta L_f^{(e)} \neq 0$ for at least one line f. As explained above, the base case is apt to take into account (anticipated) intra-zonal trade. We deliberately choose situations with intra-zonal trade as possible base cases. We know from sec. 3.3 that $r_{BC,2}^{abs,(e)}$=-0.5 describes such situations. Thus, we choose two situations that lay within the subspace of the nodal FR for this NER introduced in sec. This base case subspace is highlighted in grey in fig. 5 for reference. 3.3.

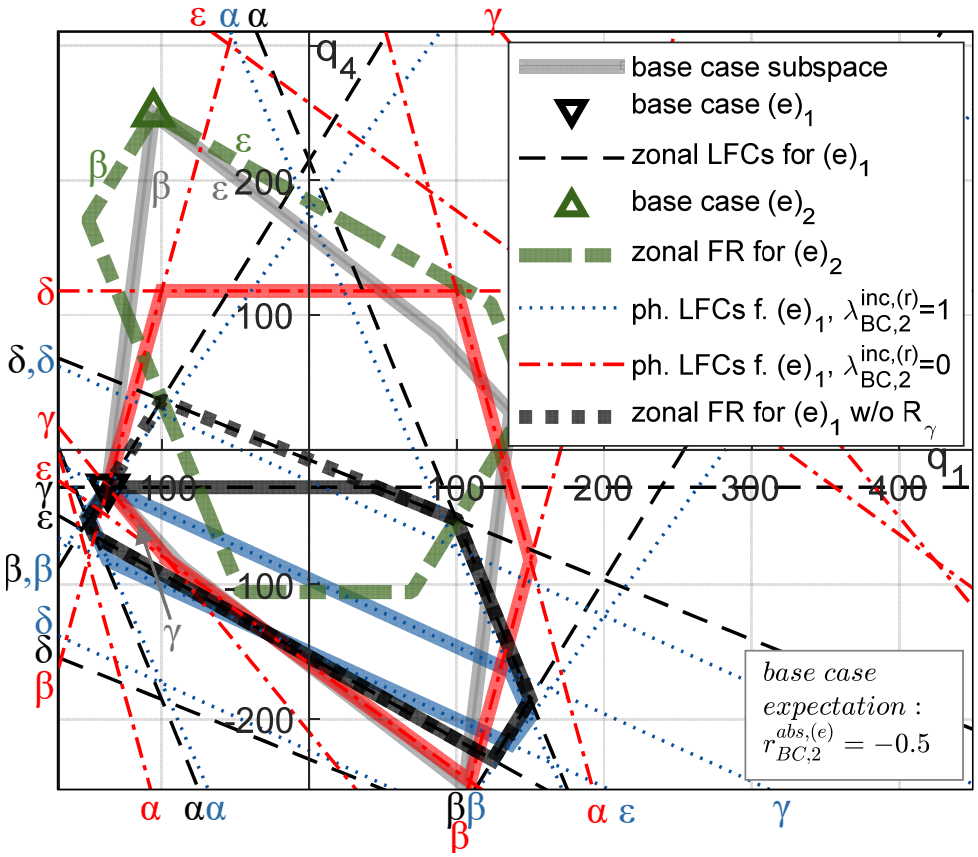

Figure 5: LFCs of the zonal and nodal EMCP for the 4-node example under a non-zero base case (for the nodal EMCP, two realizations are shown for base case $(e)_1$; for base case $(e)_2$, LFCs are not shown for lucidity).

The chosen base cases are denoted by $(e)_1$ and $(e)_2$ (indicated by the two triangles). These base cases together with the predetermined GSK $\lambda_{BC,2}^{inc,(p)}$ entirely define the zonal FRs. These zonal FRs are marked by the solid black ((e_1)) and dashed green ((e_2)) enframed areas. They can

be understood as planar cuts through the nodal FR (feasibility polyhedron). The tilt of these planar cuts is defined by $\lambda_{BC,2}^{inc,(p)}$. The offset from the origin is given by $(e)_1$ and $(e)_2$ respectively. Thus, the base case, by design, constitutes one situation in the zonal FR. In our examples, the base cases are located at the corners of the nodal FR defined by the LFCs of line pairs β/γ and β/ϵ. The corresponding LFCs are also binding in the zonal EMCP if and only if the market outcome is identical to the base case situation. Thus, if the base case represents (or, at least, is close to) the welfare-optimal dispatch situation, this welfare-optimal situation (or situations close to the welfare optimum) is part of the zonal FR.
By comparison of the zonal FRs of $(e)_1$ and $(e)_2$, it becomes apparent that the zonal FRs greatly depend on the base case - in terms of relevant LFCs, size of FRs, differences of feasible sets, etc. It is obvious that the accuracy of the base case expectation is a prerequisite for good FBMC results.
Fig. 5 also shows the LFCs for $(e)_1$ when realized GSKs differ from $\lambda_{BC,2}^{inc,(p)}$ (using the same color scheme as in fig. 4). As in sec. 3.3, the subspaces of the nodal FR are quite different. In particular, the subspace for $\lambda_{BC,2}^{inc,(r)} = 0$ is much wider than the nodal FR. This indicates the increased flexibility available to nodal EMCP due to more degrees of freedom.

As before, the zonal EMCP may hence either lead to welfare losses compared to the nodal case or require redispatch.

3.5 Considering Intra-zonal Lines

In base case $(e)_1$ in sec. 3.4, one of the LFCs of the intra-zonal line γ is binding (cf. fig. 5). From sec. 3.4, we know that this LFC is also relevant for definition of the zonal FR. If $\lambda_{BC,2}^{inc,(r)}$ is equal to $\lambda_{BC,2}^{inc,(p)}$, any dispatch situation with $q_4 > -27.85$ MW will lead to overloads of line γ. If the LFC of line γ is not considered, the zonal FR allows q_4 to exceed this limit. This is illustrated by the alternative zonal FR enframed by bold and black dotted lines. Thus, considering LFCs of internal lines can help avoiding overload situations. Nevertheless, the recourse of the zonal EMCP to prevent such overloads is limited, since only zonal net exports can be optimized, although the more effective congestion management may be the optimization of intra-zonal trade. We use our example to illustrate this.
Consider the possible trades of 100 MWh from (i) node 4 to zone BC, (ii) node 1 to zone BC and (iii) node 3 to node 2. With the FBMC power flow approximation, i.e. $\lambda_{BC,2}^{inc,(p)}$, trades (i) and (ii) result in a change of transmitted electricity through line γ of -12.5 MWh and 0 MWh respectively (cf. $A_{\gamma,1/4} - \bar{A}_{\gamma,BC}$). By contrast, the intra-zonal trade (iii) changes transmission through line γ by 62.5 MWh ($A_{\gamma,3} - A_{\gamma,2}$). Even though intra-zonal adjustments are the most effective way of managing congestion on line γ, the zonal EMCP can only optimize zonal net exports.
Analogously, the high $A_{\gamma,2}$ entails that the LFC for line γ is extremely sensitive to the intra-zonal trade expected in the base case. The above example shows that 1 MWh of additionally

expected trade from node 3 to 2 limits the exports from node 4 by additional 5 MWh. Hence, a tight upper bound of the net exports at node 4 is implemented in the zonal EMCP.
The previous statement notably holds for the effect of forecast deviations on intra-zonal trades in the base case, but it likewise constitutes a dilemma for any base case expectation with binding or even overloaded intra-zonal lines. If the true expectation of intra-zonal trades is high, the base case yields either a highly constrained or empty zonal FR. This would either imply welfare decreases or make day-ahead clearing infeasible. If the base case is adjusted to contain less intra-zonal trade, the zonal FR is less restrictive, but the zonal market clearing will result in higher intra-zonal trade (close to the true base case expectation). Thus, redispatch is the consequence. Such base case adjustments correspond to the implicit remedial actions mentioned in TSO documents [Elia 2015]. Yet, these documents address the consideration of implicit remedial actions quite vaguely and merely state that these actions can be considered as FAV. The above-described case gives a concrete example of the cause and effect of considering remedial actions in the base case.
Thus, two extreme positions regarding intra-zonal lines may be distinguished. Either they are disregarded in the zonal EMCP. Then, congestion management of these lines is not performed during the D-1 stage, which may require redispatch afterwards. Or intra-zonal lines are explicitly considered in FBMC, yet then they may strongly impede cross-zonal trade. In some cases, the impediments are so strong that base case adjustments are necessary. These adjustments at the D-2 stage then materialize as redispatch on day D. Between these extreme positions, also intermediate solutions may be chosen, namely to include only some intra-zonal lines as constraints in the EMCP. Here, the example illustrates a prerequisite for a meaningful inclusion of intra-zonal line constraints: that the corresponding power flows are sufficiently sensitive to variations in cross-zonal trade (cf. sec. 2.2.5 for the threshold established by TSOs). The effects of this selection are investigated in Part II [Felling et al. 2019] using the large-scale model.

3.6 Use and Effects of FRMs

In order to consider the uncertainties of the FBMC process, Entso-E procedures consider the incorporation of FRMs [Amprion et al. 2014], which have already been briefly introduced in sec. 2.2. By construction, an FRM causes a parallel shift of the zonal LFCs reducing the FR. For the sake of clarity, we now move back to our example in sec. 3.3 (base case $(e)_0$). Furthermore, we suppose that redispatch is to be avoided completely. Under this presumption, FRMs need to be chosen in a way that the zonal FR only contains technically feasible solutions. If we assume possible realizations $\lambda_{BC,2}^{inc,(r)} \in [0,1]$, FRMs need to be chosen in a way that they shift the LFCs to the most critical realization. Fig. 6 illustrates the resulting FR of the zonal EMCP with FRMs (still assuming $\lambda_{BC,2}^{(e)}$=0.8). For brevity, we only contrast the zonal FR to the subspace of the nodal FR for $\lambda_{BC,2}^{inc,(r)}$=0 in fig. 6. However, for the derivation of required FRMs, we have also taken into account $\lambda_{BC,2}^{inc,(r)}$=1.
The red areas highlight solutions of the zonal EMCP which, without consideration of FRMs,

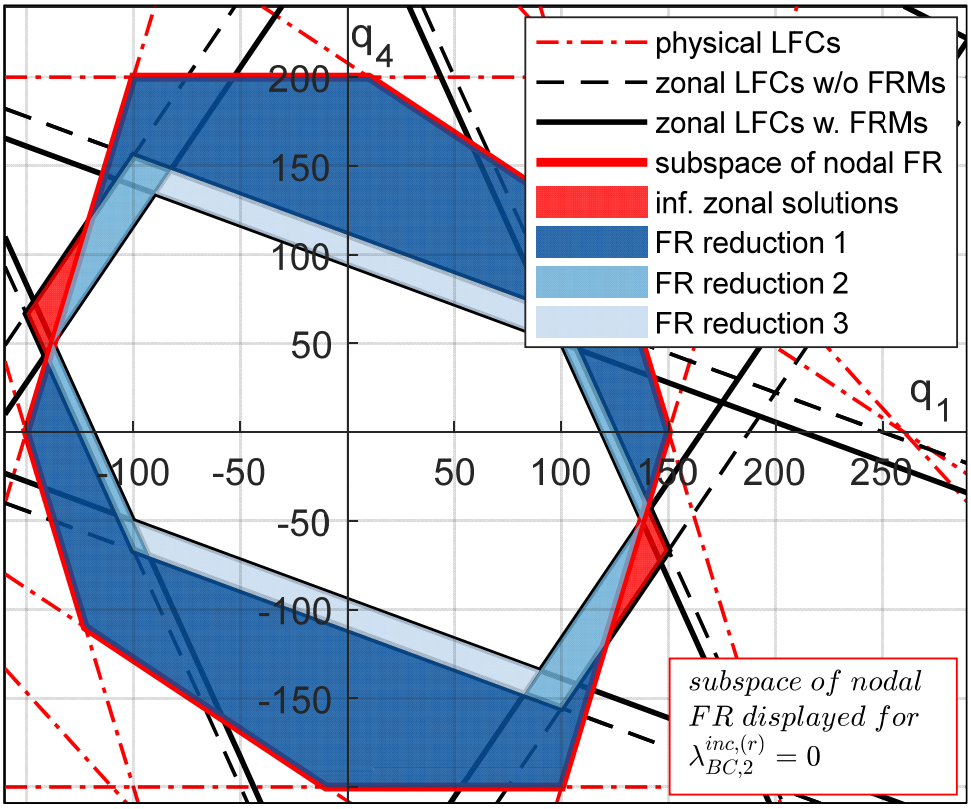

Figure 6: LFCs of the zonal and nodal EMCP for the 4-node example under a zero base case (for the nodal EMCP, only one realizations, $\lambda_{BC,2} = 0$, is shown).

would be technically infeasible at $\lambda_{BC,2}^{inc,(r)}$=0. All blue areas depict the set of technically feasible solutions which, due to the zonal market design, are not part of the FR of the zonal EMCP. Thereof, the solutions indicated by dark blue areas (FR reduction 1) are excluded due to the distortion of the zonal FR compared to the nodal subspace. The solutions in the light blue areas are excluded due to the use of FRMs. FR reduction 2 is due to required contingency margins in case of $\lambda_{BC,2}^{inc,(r)}$=0, FR reduction 3 is due to making provision for $\lambda_{BC,2}^{inc,(r)}$=1. If the optimal solution of the nodal EMCP is located in any of the blue areas, this will cause a loss of welfare. More generally, even if the forecasts of the GSKs and of the market outcome were perfect, the result of the zonal EMCP would still be suboptimal as long as the optimal solution contains a congested line being subject to an FRM. In practice, FRMs are yet not chosen as to avoid all possible redispatch. TSOs rather perform a statistical analysis [Amprion et al. 2014]. However, the reduction of the FR happens analogously.

3.7 On Small-Scale and Large-Scale Systems

The previous sections have analyzed the essential FBMC elements. We have explained their benefits and shortcomings. While such analyses are most suitable to create awareness of persisting inefficiencies in this state-of-the-art zonal market design, the analyses of small-scale systems have some implications. Notably, with a system containing few nodes, PTDFs are relatively high ($A_{\gamma,2}$=0.625 in sec. 3.1 as opposed to a mean absolute PTDF value of 0.007 in our large-scale model), and PTDFs of the same line are very different for individual nodes within the same zone. Thus, loading of transmission lines is highly sensitive in our stylized model (cf. fig. 4), and effects may consequently be overdrawn. To some extent, all stylized models have these common characteristics that differ from the real world (cf. [Bjørndal and Jörnsten 2001; Bjørndal et al. 2003; Ehrenmann and Smeers 2005; Bjørndal and Jörnsten 2007; Oggioni and Smeers 2013; Grimm et al. 2016; Grimm et al. (2) 2016]). Thus, small-scale models are useful to reveal weaknesses of MC procedures, but one should reflect on their results. In order to assess whether inefficiencies of FBMC are meaningful, large-scale models are required that reproduce real-world system behavior. The next section presents a comprehensive model framework that allows such reproduction and quantification.

4 Large-Scale Modeling Approach

Fig. 7 provides a schematic flow chart of the developed model framework. In general, the design approach has been to make use of proven models, extend these by new functions and features and develop a customized data handling environment. The use of several specialized models allows reproducing real-world system behavior and processes to a high level of detail.

4.1 Consistent input data generation

The first model step is the generation and structuring of input data for the grid simulation as well as for the market simulation. It produces hourly time series of the so-called vertical load (i.e. electric demand minus renewables-based (RES) infeed and minus production of small-scale power plants) at each node. Especially power flow assessments require these input data at nodal level, while, for market simulations, the data are aggregated to zonal values. Hourly regional demand values are calculated in a top-down approach; i.e. demand is split into different sectors (industry, service sector and households) and distributed to regions based on their share of sector-specific gross value added or population respectively. Regional PV and wind infeeds are calculated in a bottom-up approach, using characteristic infeed profiles for each region based on measured data from local plants (PV) or simulated data (wind) using wind speed data [DWD 2017] at the position of known local wind farms as well as their power curves and hub heights projected to the simulated year. This characteristic profile is scaled with the forecast regional installed capacity. Generally, all individual time series are determined at the third level of Eurostat's NUTS classification (i.e. resulting in 642 regions×3 time series×8,760 h/a=16.9 million values) and then mapped to grid nodes. Offshore wind time series constitute an exception to this rule. They are calculated taking into account single wind parks. The Matlab-based program is a greenfield development made for combined grid and market modeling. It is optimized for handling large amounts of data and automatically sourcing the required data from the used meteo data base. A detailed description is given in [Osinski et al. 2016].

4.2 Capacity Allocation (D-2)

The second model step is the capacity allocation. Such grid-focused processes are best handled in specialized tools like the open-source program MATPOWER [Zimmermann et al. 2011]. This program has the advantage that certain functions are readily available and extensively tested (cf. [Zimmermann and Murillo-Sánchez 2018] for comprehensive documentation). Using an open-source program has allowed us to develop customized functions. Subsequently, we provide some examples.

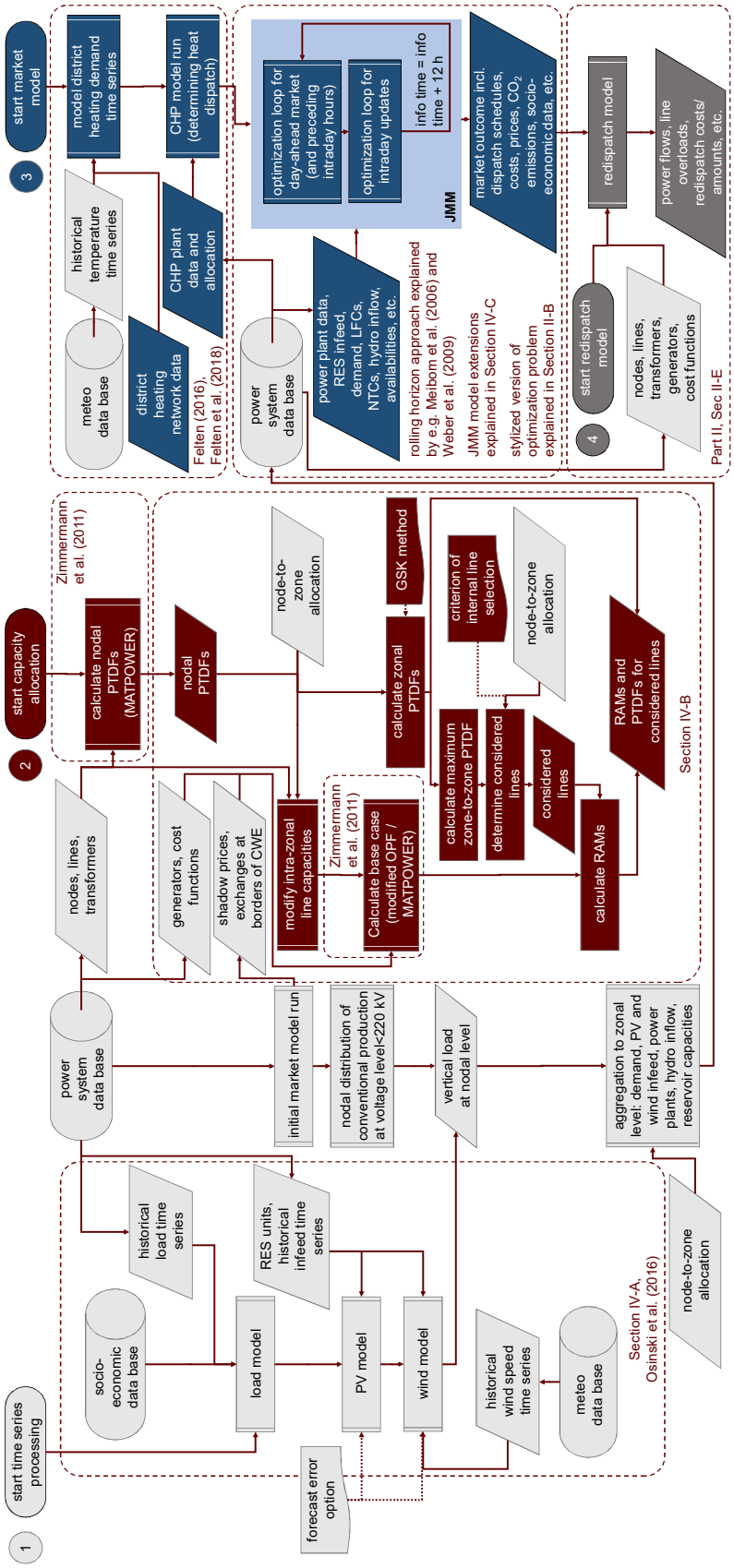

Figure 7: Flow chart of the developed model framework, sketching a typical FBMC assessment (D-2 to D stage). Multiple elements signify identical elements.

Zonal PTDFs Zonal PTDFs can be calculated using eq. 11 given the nodal PTDFs and GSKs. Nodal PTDFs can be calculated in MATPOWER based solely on the input parameters of the regarded grid (topology and susceptances). GSKs depend on the chosen calculation procedure (cf. sec. 2.2.5), power system data and on the node-to-zone allocation. Hence, our program accesses our power system data base and replicates the TSO procedures. These zonal PTDFs are then used for various purposes: RAM calculation, D-1 market clearing (cf. sec. 4.3) and for the selection of intra-zonal lines to be considered in the EMCP (cf. sec. 2.2.5).

Intra-zonal line selection For the selection of intra-zonal lines, we have implemented the 5% threshold proposed by TSOs (cf. [Amprion et al. 2014]). Moreover, in Part II [Felling et al. 2019], we argue that this threshold is not suitable for any given price zone configuration. Thus, we have defined and implemented further selection criteria. These alternative selection procedures and their effects in terms of MC are explained in detail in Part II [Felling et al. 2019].

Base case and RAMs The calculation of the base case is somewhat more sophisticated. As explained in sec. 2.2.5, the base case constitutes a best D-2 estimate for the market outcome. However, the market outcome depends on the FBMC parameters. [ACM et al. 2015] call this a circular problem. TSOs have found a workaround by using a reference day. This seems expedient if especially two conditions are fulfilled. First, the number of FBMC price zones needs to be limited. Currently, this is the case with CWE containing four price zones. This aspect results in a small set of "likely corners" of the zonal FR, which reduces complexity of choosing such a reference day. Second, sufficient and consistent historical data needs to be available. For model-based assessments, however, both conditions are hardly fulfilled. In particular, such models are often used to analyze alternative market designs, policy choices and future scenarios. This includes possibilities like a drastically higher number of price zones or structural changes in fundamental factors (e.g. RES expansion, conventional capacity decrease, etc.). Thus, we use a slightly different procedure to establish the best D-2 estimate. For doing so, we use the optimal power flow (OPF) function of MATPOWER [Zimmermann and Murillo-Sánchez 2018]. With constant marginal costs for each generator, this OPF corresponds to the nodal EMCP in sec. 2.1, and we refer to this nodal EMCP to explain our estimation of the base case. In the nodal EMCP, line capacities C_f of intra-zonal lines can be increased to a level where the corresponding LFCs never become binding. Effectively, this is the same as reducing the set F_x. If doing so, only inter-zonal lines are relevant and zones are free of congestion. Hence, this modified EMCP describes a zonal clearing. Thereby, we use the same data set as for detailed grid assessments with the exception of the C_f modification for intra-zonal lines. The result is a reasonable estimate of a zonal market outcome.[7] As one additional option, we can use different accuracies

[7] The nodal EMCP in sec. 2.1 obviously contains some simplifications compared to a real-world zonal clearing, e.g. the disregard of intertemporal constraints of power plants. However, TSO procedures neither consider such constraints explicitly.

for the RES infeed forecast. This influences the (vertical) load (i.e. d_i) in the EMCP/OPF and, thus, induces inaccuracies in the base case expectation. Thus, our adjusted OPF yields a reasonable estimate of a zonally organized market, possibly considering D-2 forecast errors.

Having determined the base case and the zonal PTDFs, RAMs can be calculated pursuant to eq. 12 and 13. For this calculation, several options for the FRM levels can be chosen. We explain the options in Part II [Felling et al. 2019], where we also perform respective sensitivity analyses. A typical data set of the capacity allocation model contains approx. 2,200 nodes, 3,500 lines and 700 transformers. This entails around 9 million nodal PTDF matrix elements. Using the 5% threshold and countries as price zones, the number of zonal PTDF elements is condensed to around 1,300. The zonal PTDFs and corresponding RAMs are handed over to the market model.

4.3 Day-ahead and intraday market clearing

The third model step replicates the market processes. Prior to simulating the actual bidding on electricity markets, the constraints from combined heat and power (CHP) provision need to be determined. This is important as many European countries are characterized by high shares of CHP and as heat scheduling typically takes place ahead of electricity market clearing (cf. [Nielsen et al. 2016; Varmelast 2018]). Therefore, we use a separate CHP model. In a first step, this tool models the heat demand of district heating grids. In a second step, it determines the heat extraction from CHP plants, which then can be translated into minimum and maximum electricity generation bounds for these units. The model is documented in [Felten 2016; Felten et al. 2017] and has proven suitable for power system planning [50Hertz Transmission GmbH et al. 2018]. The constraints determined with the CHP model are handed over to the used electricity market model, the JMM, which replicates the real-world electricity markets. The JMM is a detailed scheduling model which has repeatedly been used for academic and industrial purposes (e.g. in [Tuohy et al. 2009; Meibom et al. 2011; Trepper et al. 2015]). The model is based on the assumption of a competitive market and (as used here) inelastic demand. Thus, the market outcome corresponds to the result of a central cost minimization. The basic principle of the EMCP is similar to the one of the stylized EMCP in eq. 6 to 10. Nonetheless, there are manifold aspects which either diverge from or add much more details to the simple formulations in eq. 6 to 10. As one indicator for the complexity increase from the stylized EMCP to the JMM, the number of constraints of the optimization problem can be regarded: The simple formulation in sec. 2.2 has 4 types of constraints (eq. 7 to 10), the JMM has more than 40 constraint types. Another metric is the size of the set of power plants. While, for the stylized EMCP, we have simply assumed 4 power plant capacities, a typical JMM run takes into account around 17,000 power plants, grouped into around 700 plant classes, and their various constraints. From sec. 4.2, we know that a typical PTDF matrix of the JMM has 1,300 values. The simple zonal EMCP considers 15 PTDFs (3 zones, 5 lines). For brevity, the most relevant

Table 3: Most relevant differences between simplified EMCP in eq. 6 to 10 and the general JMM formulation (except for LFCs).

eq. 6-10	**JMM**	**description of differences in the used JMM configuration**
–	t	Instead of considering one specific situation, the JMM considers all hours of the year. In addition, a rolling horizon approach is used to model day-ahead and intraday markets. The set of time stamps which are considered jointly for each day-ahead clearing (or intraday adjustments) is denoted T^{opt}.
g_i	$g_{u,t}$	Generation per unit (or unit groups, i.e. power plants of the same type, with similar age and within the same region (price zone)).
$c_i(g_i)$	$c_u(g_{u,t})$	The nodal variable-cost function is broken down into individual variable-cost functions per unit / unit group. These functions consider fuel usage (which increases linearly with generation plus a fixed term for operating units), fuel costs, CO_2 costs, variable operation and maintenance costs and start-up cost. For hydro power plants, shadow prices for hydro reservoir and pump storage content are used instead of fuel and CO_2 costs.
$g_i \geq 0$	$g_{u,t} - g_{u,t}^{spin,-} \geq g_{u,t}^{min}$	Minimum generation constraints for units are considered. In particular, these take into account technical minimum generation (for operating units) and must-run constraints from CHP plant operation. The thermal output is calculated with a separate CHP model (cf. [Felten 2016; Felten et al. 2017]) and electrical constraints result from the operational map of CHP plants in the JMM (which, for brevity, are summarized as $g_{u,t}^{min/max}$). In addition to actual power generation $g_{u,t}$, negative spinning reserve power $g_{u,t}^{spin,-}$ is considered (related reserve constraints are given in [Meibom et al. 2006; Weber et al. 2009]).
$g_i \leq g_i^{max}$	$g_{u,t} + g_{u,t}^{spin,+} + g_{u,t}^{nonsp,+} \leq g_{u,t}^{max}$	Maximum generation constraints are considered in more detail. The time dependency results from varying availabilities and CHP constraints (cf. above). In addition, $g_{u,t}^{spin,+}$ and $g_{u,t}^{nonsp,+}$ stand for capacity reservations that have to be made for positive spinning and non-spinning reserves respectively (related reserve constraints are given in [Meibom et al. 2006; Weber et al. 2009]).
$\bar{q}_z$	$\sum_{z'} e_{z,z',t} - \sum_{z} e_{z',z,t}$	Instead of net exports, bilateral exchanges $e_{z,z',t}$ from price zone z to zone z' are modeled. This has the advantage of a more convenient combined modeling of FBMC and NTC-based MC (depending on the MC definition for each price zone, cf. eq. 16 to 19).
d_z	$\sum_{i \in I_z} d_{i,t}$	Consistent nodal and zonal demand time series are used (generated by the vertical load model and being input for both the JMM and the grid model, cf. sec. 4.1).
–	$\sum_{i \in I_z} g_{i,t}^{res}$	Consistent nodal and zonal infeed time series from non-dispatchable RES, being generated by the vertical load model and being input for both the JMM and the grid model. RES infeed can be curtailed at high penalties, but the relevant terms are not displayed here.
–	reservoir constraints	Intertemporal constraints linking reservoir filling levels and calculating shadow prices from long-term strategic reference filling levels are implemented (cf. description in [Meibom et al. 2006; Weber et al. 2009])
–	minimum downtime	Minimum downtime constraints specific to each unit / unit group are used (cf. [Meibom et al. 2006; Weber et al. 2009]).
–	minimum operation	Minimum operating time constraints specific to each unit / unit group are used (cf. [Meibom et al. 2006; Weber et al. 2009]).

real-world model features - in extension to the stylized EMCP - are listed in table 3. For a more comprehensive description, the reader is referred to [Meibom et al. 2006]. As can be seen in table 3, the constraints implemented in the JMM are much more complex than those used

for theoretical analyses as in sec. 2 or in [Bjørndal and Jörnsten 2001; Bjørndal et al. 2003; Ehrenmann and Smeers 2005; Bjørndal and Jörnsten 2007; Androcec and Krajcar 2012; Neuhoff et al. 2013; Oggioni and Smeers 2013; Grimm et al. 2016; Grimm et al. (2) 2016].

With regard to JMM developments, the must-run constraints of CHP plants have been implemented in the course of the present work. This is said for the sake of completeness, as the constraints differ from [Meibom et al. 2006], but is not in the focus of this paper. A model development that is in the focus of this paper and constitutes a major contribution is the consideration of FBMC in a large-scale market model. This statement especially refers to three aspects. First, we make use of input data from large-scale yet specialized and very detailed models. Another choice could have been to implement a simplified (e.g. aggregated) grid model in the JMM. This alternative choice could have reduced model interfaces whilst entailing losses in accuracy. Therefore, we have focused on interface design with the goal of most realistic FBMC constraint parametrization. Second, large-scale modeling does not only refer to CWE. Price zones in CWE are not isolated from the other European markets. A common regional scope of the JMM comprises entire continental Europe plus Scandinavia, UK and Ireland and excl. Russia, Ukraine and the Baltics. Thus, the effect of interlinked European markets is reproduced. Third, until now, FBMC is only carried out between price zones in CWE. MC with and between markets outside of CWE is still performed by means of NTC-based MC. The JMM developments have taken this into account. As part of the case definition of the JMM, zones can be assigned to the subset Z_{FB}. The commercial exchanges between pairs of these zones ($(z, z') \in Z_{FB} \times Z_{BF}$) are then subject to FBMC. Cross-zonal exchanges between the remaining zone pairs ($(z, z') \in \{\{Z \times Z\} \setminus \{Z_{FB} \times Z_{BF}\}\}$) are managed on basis of NTCs. This user-defined allocation of zones to the set Z_{FB} does not only allow to model the current set-up, it also enables us to simulate future scenarios where further price zones use FBMC. The resulting LFCs are given in eq. 16 to 18. They are similar to the ones of the simple EMCP (eq. 6 to 10). Yet, the implementation in the JMM mainly differs in regard to three aspects: First, constraints apply for each hour of the optimization loop ($t \in T^{opt}$). The optimization loops move forward in a receding horizon approach (cf. [Meibom et al. 2006]), so that a complete year is simulated. With the JMM containing intertemporal constraints, also the LFCs for different time stamps interfere. Furthermore, depending on the base case expectation, the RAMs vary for different time stamps. Second, lines may not only be used for scheduled power exchanges on the day-ahead market. Intraday adjustments of exchanges may change (zonally-approximated) line loadings.[8] Similarly, part of the line capacities may be reserved for use of cross-border nonspinning reserves. The third major difference has been explained above: The distinction between zones being coupled based on NTCs and zones using FBMC. This entails one formal difference

[8] Note that we model FB-like constraints to also apply for intraday MC. This modeling slightly differs from real-world implementation.

to eq. 7. Our formulation uses bilateral exchanges $e_{z,z',t}$ instead of net exports $\bar{q}_z$. This simply allows us to use the established variables of bilateral exchanges for both MC methods.

$$e_{z,z',t} = e^{DA}_{z,z',t} + \Delta e^{ID,+}_{z,z',t} - \Delta e^{ID,-}_{z,z',t} + e^{nonsp,+}_{z,z',t} \quad \forall\, t \ \in T^{opt},\ \forall\, (z,z') \in Z \times Z \tag{16}$$

$$R^{nsfd}_{f,t} \leq \sum_z \bar{A}_{f,z,t} \left(\sum_{z'} e_{z,z',t} - \sum_{z'} e_{z',z,t}\right) \leq R^{sfd}_{f,t} \quad \forall\, f \in F_{cb}, \forall\, t \in T,\ \forall (z,z') \in Z_{FB} \times Z_{FB} \tag{17}$$

$$0 \leq e_{z,z',t} \leq e^{max}_{z,z',t} \quad \forall t \ \in T^{opt},\ \forall\, (z,z') \in \{\{Z \times Z\} \setminus \{Z_{FB} \times Z_{FB}\}\} \tag{18}$$

$$e^{DA}_{z,z',t}, \Delta e^{ID,+}_{z,z',t}, \Delta e^{ID,-}_{z,z',t}, e^{nonsp,+}_{z,z',t} \geq 0 \quad \forall\, t \ \in T^{opt},\ \forall\, (z,z') \in Z \times Z \tag{19}$$

Eq. 16 thereby gives the components of the bilateral exchange variable $e_{z,z',t}$, eq. 17 provides the LFCs for FB-coupled price zones, eq. 18 constitutes the NTC (and non-negativity) constraint for $e_{z,z',t}$, and eq. 19 summarizes the nonnegativity constraints of the components of $e_{z,z',t}$.

4.4 Redispatch

The model framework contains one more essential step - the modeling of redispatch (cf. fig. 7). Without an assessment of redispatch quantities and costs, a significant part would be missing in FBMC assessments. This is especially important under consideration of the drastic rise of redispatch (incl. RES curtailment) within CWE during recent years [Federal Ministry for Economic Affairs and Energy 2018]. A detailed model description is given in Part II [Felling et al. 2019].

5 Conclusion

This paper provides two major contributions in terms of the understanding and assessment of FBMC. First, it analyzes the causes and effects of all essential FBMC elements – namely, the GSKs, the base case and intra-zonal LFCs – based on a small-scale example. On the one hand, we have been able to show that TSOs have found interesting answers to problems envisaged during the early discussions of MC [Ehrenmann and Smeers 2005]. Especially, the base case constitutes a means for taking into account intra-zonal trade and, thereby generally being able to shift the zonal FR close to a welfare optimal dispatch. However, fundamental shortcomings of zonally organized markets remain. E.g. the ex-ante determination of zonal PTDFs by use of GSKs makes LFCs inaccurate. In almost all cases with scarce exchange capacities, this entails welfare losses and/or redispatch. While the consideration of intra-zonal LFCs can prevent line overloads, we show that the effectiveness of managing congestion of intra-zonal lines in FBMC is clearly inferior to a nodal congestion management. This calls for price zone delimitations oriented towards the most congested lines. The second main contribution of this paper is the introduction of a large-scale model framework that is able to assess real-world power systems using FBMC. The framework is founded on several detailed large-scale models - notably MATPOWER and the JMM (incl. its CHP tool). Additional functions/features have been implemented into these models to replicate the FBMC capacity allocation process and to consider the relevant constraints for market clearing. This includes the combined consideration of FBMC and NTC-based MC. These functions are programmed in a general manner, so that they allow for sensitivity assessments of FBMC elements. Part II of this two-part paper takes up both components of this paper. In particular, the effects of the FBMC elements can also be detected in the large-scale model framework and can eventually be quantified.

References

50Hertz Transmission GmbH, Amprion GmbH, TenneT TSO GmbH, and TransnetBW GmbH (2018). *Szenariorahmen für den Netzentwicklungsplan Strom 2030 (Version 2019)*. Entwurf der Übertragungsnetzbetreiber (cit. on p. 21).

ACM et al. (2015). *Position Paper of CWE NRAs on Flow-Based Market Coupling* (cit. on p. 20).

Amprion, APX, Belpex, Creos, Elia, EpexSpot, RTE, Tennet, TransnetBW (2014). *Documentation of the CWE FB MC solution as basis for the formal approval-request*. Tech. rep. (cit. on pp. 7 sq., 15 sq., 20).

Amprion et al. (12/08/2014). *Communication to Market Participants - CWE Flow-Based Market Coupling* (cit. on p. I).

Androcec, I. and Krajcar, S. (2012). "Methodology of market coupling/splitting for efficient cross-border electricity trading". In: *2012 9th International Conference on the European Energy Market*, pp. 1–8 (cit. on pp. 2, 23).

Bjørndal, M. and Jörnsten, K. (2001). "Zonal pricing in a deregulated electricity market". In: *The Energy Journal*, pp. 51–73 (cit. on pp. 2 sq., 17, 23).

Bjørndal, M. and Jörnsten, K. (2007). "Benefits from coordinating congestion management—The Nordic power market". In: *Energy policy* 35.3, pp. 1978–1991 (cit. on pp. 2, 17, 23).

Bjørndal, M., Jørnsten, K., and Pignon, V. (2003). "Congestion Management in the Nordic Power Market - Counter Purchase and Zonal Pricing". In: *Journal of Network Industries* 4.3, pp. 271–291 (cit. on pp. 2, 17, 23).

Deutscher Wetterdienst (DWD) (2017). *Regional Model COSMO-EU*. URL: `https://www.dwd.de/EN/research/weatherforecasting/num_modelling/01_num_weather_prediction_modells/regional_model_cosmo_eu.html` (visited on 09/20/2017) (cit. on p. 18).

Dierstein, C. (2017). "Impact of Generation Shift Key determination on flow based market coupling". In: *14th International Conference on the European Energy Market (EEM), Dresden* (cit. on p. 8).

Ehrenmann, A. and Smeers, Y. (2005). "Inefficiencies in European congestion management proposals". In: *Utilities policy* 13.2, pp. 135–152 (cit. on pp. 2 sq., 17, 23, 25).

Elia (01/01/2017). *Loop flows calculation*. URL: `http://www.elia.be/en/grid-data/interconnections/Loopflows` (visited on 11/17/2018) (cit. on p. 12).

Elia System Operator S.A. (2015). *Implementation of day-ahead flow-based market coupling in the CWE region*. Tech. rep. (cit. on pp. 8, 15).

Entso-E (09/2016). *Entso-E Generation and Load Shift Key Implementation Guide*. Brussels, Belgium (cit. on p. 7).

Entso-E (02/05/2018). *First edition of the bidding zone review - draft version for public consultation* (cit. on pp. I, 3, 7).

Federal Ministry for Economic Affairs and Energy (2018). *Sechster Monitoring-Bericht zur Energiewende*. URL: `https://www.bmwi.de/Redaktion/DE/Publikationen/Energie/`

sechster-monitoring-bericht-zur-energiewende.html (visited on 11/18/2018) (cit. on p. 24).

Felling, T., Felten, B., Osinski, P., and Weber, C. (2019). "Flow-Based Market Coupling Revised - Part II: Assessing Improved Price Zone Configurations in Central Western Europe". In: *Energy Economics* XX.1, pp. X–X (cit. on pp. 1, 15, 20 sq., 24).

Felten, B. (06/20/2016). *CHP Plant Operation and Electricity Market Prices – Analytical Insights and Large-Scale Model Application*. 39th IAEE International Conference (cit. on pp. 21 sq.).

Felten, B., Baginski, J. P., and Weber, C. (2017). *KWK-Mindest- und Maximaleinspeisung - Die Erzeugung von Zeitreihen für die Energiesystemmodellierung*. HEMF Working Paper No. 10/2017. URL: https://papers.ssrn.com/sol3/papers.cfm?abstract_id=3082858 (visited on 12/11/2017) (cit. on pp. 1, 21 sq.).

Finck, R., Ardone, A., and Fichtner, W. (2018). "Impact of Flow-Based Market Coupling on Generator Dispatch in CEE Region". In: *2018 15th International Conference on the European Energy Market (EEM), Lódz, PL, June 27–29, 2018*. 37.06.01; LK 01. IEEE, Piscataway, NJ, pp. 1–5 (cit. on p. 1).

Grimm, V. et al. (2) (2016). "Transmission and generation investment in electricity markets: The effects of market splitting and network fee regimes". In: *European Journal of Operational Research* 254.2, pp. 493–509 (cit. on pp. 2, 17, 23).

Grimm, V., Martin, A., Weibelzahl, M., and Zöttl, G. (2016). "On the long run effects of market splitting: Why more price zones might decrease welfare". In: *Energy Policy* 94, pp. 453–467 (cit. on pp. 2 sq., 17, 23).

Jegleim, B. (2015). *Flow Based Market Coupling*. Master thesis. URL: http://hdl.handle.net/11250/2368078 (visited on 11/07/2018) (cit. on p. 3).

Marjanovic, I., v. Stein, D., van Bracht, N., and Moser, A. (2018). "Impact of an Enlargement of the Flow Based Region in Continental Europe". In: *2018 15th International Conference on the European Energy Market (EEM)*, pp. 1–5 (cit. on p. 1).

Meibom, P. et al. (2011). "Stochastic Optimization Model to Study the Operational Impacts of High Wind Penetrations in Ireland". In: *IEEE Transactions on Power Systems* 26.3, pp. 1367–1379 (cit. on p. 21).

Meibom, P. et al. (2006). *Wilmar joint market model. Documentation*. Tech. rep. Risø National Laboratory (cit. on pp. 1, 22 sq.).

Morin, T. (2016). *Statistical Study and Clustering of the Critical Branches Defining the Market Coupling in the Central West Europe Zone*. Master thesis. URL: http://www.diva-portal.org/smash/record.jsf?pid=diva2%3A930849&dswid=-5954 (visited on 11/07/2018) (cit. on p. 3).

Neuhoff, K. et al. (2013). "Renewable electric energy integration: quantifying the value of design of markets for international transmission capacity". In: *Energy Economics* 40, pp. 760–772 (cit. on pp. 2 sq., 23).

Nielsen, M.G. et al. (2016). "Economic valuation of heat pumps and electric boilers in the Danish energy system". In: *Applied Energy* 167, pp. 189–200 (cit. on p. 21).

Oggioni, G. and Smeers, Y. (2013). "Market failures of Market Coupling and counter-trading in Europe: An illustrative model based discussion". In: *Energy Economics* 35, pp. 74–87 (cit. on pp. 2, 17, 23).

Osinski, P., Becker, R., and Weber, C. (09/09/2016). *Regional modelling of electric load and renewable infeed time series in Europe* (cit. on p. 18).

Plancke, G. et al. (2016). "Efficient use of transmission capacity for cross-border trading: Available Transfer Capacity versus flow-based approach". In: *2016 IEEE International Energy Conference (ENERGYCON)*, pp. 1–5 (cit. on pp. 3, 10).

Schönheit, D. and Sikora, R. (2018). "A Statistical Approach to Generation Shift Keys". In: *2018 15th International Conference on the European Energy Market (EEM)*, pp. 1–6 (cit. on p. 8).

Sebestyén, M., Divenyi, D., and Sőrés, P. (2018). "An Enhanced Calculation Method of Generation Shift Keys in Flow Based Market Coupling". In: *2018 15th International Conference on the European Energy Market (EEM)*, pp. 1–5 (cit. on p. 1).

Trepper, K., Bucksteeg, M., and Weber, C. (2015). "Market splitting in Germany – New evidence from a three-stage numerical model of Europe". In: *Energy Policy* 87, pp. 199–215 (cit. on p. 21).

Tuohy, A. et al. (2009). "Unit Commitment for Systems With Significant Wind Penetration". In: *IEEE Transactions on Power Systems* 24.2, pp. 592–601 (cit. on p. 21).

Van den Bergh, K., Boury, J., and Delarue, E. (2016). "The Flow-Based Market Coupling in Central Western Europe: Concepts and definitions". In: *The Electricity Journal* 29.1, pp. 24–29 (cit. on p. 3).

Varmelast (2018). *Heating plans*. URL: `https://www.varmelast.dk/en/heating-plans` (visited on 11/18/2018) (cit. on p. 21).

Weber, C. et al. (2009). "WILMAR - a stochastic programming tool to analyse the large scale integration of wind energy". In: *Optimization in the Energy Industry*. New York: Kallrath, J. et al. (cit. on pp. 1, 22).

Wyrwoll, L., Kollenda, K., Müller, C., and Schnettler, A. (2018). "Impact of Flow-Based Market Coupling Parameters on European Electricity Markets". In: *2018 53rd International Universities Power Engineering Conference (UPEC)*, pp. 1–6 (cit. on p. 1).

Xie, J. and Hong, T. (2016). "GEFCom2014 probabilistic electric load forecasting: An integrated solution with forecast combination and residual simulation". In: *International Journal of Forecasting* 32.3, pp. 1012–1016 (cit. on p. 7).

Ziel, F. and Liu, B. (2016). "Lasso estimation for GEFCom2014 probabilistic electric load forecasting". In: *International Journal of Forecasting* 32.3, pp. 1029–1037 (cit. on p. 7).

Zimmermann, R., Murillo-Sánchez, C., and Thomas, R. (2011). "MATPOWER: Steady-State Operations, Planning and Analysis Tools for Power System Research and Education". In: *IEEE Transactions on Power Systems* 26.1, pp. 12–19 (cit. on pp. 1, 4, 18).

Zimmermann, R. and Murillo-Sánchez, C. (10/31/2018). *Matpower User's Manual Version 7.0b1*. Power System Engineering Research Center. URL: `http://www.pserc.cornell.edu/matpower/` (visited on 11/18/2018) (cit. on pp. 18, 20).

Acknowledgements

This research has partly been funded by the Federal Ministry of Economics and Technology (BMWi) of Germany within the framework of the joint project "KoNeMaSim – Kopplung von Netz- und Marktsimulationen für die Netzplanung" (project number 03ET7526). The authors gratefully acknowledge the financial support.

Correspondence

Björn Felten
Research Associate
House of Energy Markets and Finance
University of Duisburg-Essen, Germany
Universitätsstr. 12, 45117 Essen
Tel. +49 201 183-3389
Fax. +49 201 183-2703
E-Mail bjoern.felten@uni-due.de

Tim Felling
Research Associate
House of Energy Markets and Finance
University of Duisburg-Essen, Germany
Universitätsstr. 12, 45117 Essen
Tel. +49 201 183-6706
Fax. +49 201 183-2703
E-Mail tim.felling@uni-due.de

Paul Osinski
(Corresponding Author)
Research Associate
House of Energy Markets and Finance
University of Duisburg-Essen, Germany
Universitätsstr. 12, 45117 Essen
Tel. +49 201 183-6713
Fax. +49 201 183-2703
E-Mail paul.osinski@uni-due.de

Prof. Dr. Christoph Weber
Teaching Professor
House of Energy Markets and Finance
University of Duisburg-Essen, Germany
Universitätsstr. 12, 45117 Essen
E-Mail christoph.weber@uni-due.de